

MODELING COASTAL CURRENTS AND SEDIMENT TRANSPORT

by

Y. Peter Sheng¹
and
H. Lee Butler²

ABSTRACT

An efficient three-dimensional model of coastal currents and sediment transport has been developed. Simulations of tide- and wind-driven currents and sediment transport in the Mississippi Sound are presented. Results of a laboratory study on settling, resuspension, and deposition of sediment are briefly described. Wave effect on sediment resuspension is also addressed.

INTRODUCTION

Sediment transport in shallow coastal waters is an important coastal engineering problem. Many coastal waters, e.g. the Mississippi Sound, are receiving greater environmental concern due to increasing utilization of their resources, including dredging of shipping channels and disposal of dredged materials. To develop a regional plan of dredged material disposal alternatives, one should not only be concerned with the short-term fate of dredged material at specific sites, but more importantly the subsequent resuspension, transport, and deposition of sediment due to combined current and wave actions, particularly during the sporadic high-energy events.

The various physical processes that can affect the distribution of sediment in a coastal environment are shown in Figure 1. Definitive quantitative understanding of the various processes is crucial to the success of any large-scale model. Recent improvements in numerical estimation of currents and waves and the increased availability of field data and satellite imageries has made it feasible to carry out meaningful large-scale simulation studies of sediment transport events (e.g. Sheng and Lick, 1979; Sheng, 1980). In this paper, we highlight a systematic study of the sediment transport in the shallow coastal waters of the Mississippi Sound and adjacent continental shelf waters in the Gulf of Mexico.

¹Aeronautical Research Associates of Princeton, Inc., P.O. Box 2229, Princeton, NJ 08540 U.S.A.

²Wave Dynamics Division, Hydraulics Laboratory, U.S. Army Engineer Waterways Experiment Station, P.O. Box 631, Vicksburg, MS 39180 U.S.A.

In the following, a three-dimensional hydrodynamic model will be presented first, followed by a realistic simulation of tide- and wind-driven currents in the Mississippi Sound and adjacent shelf waters. Transport, resuspension, and deposition of cohesive sediments are then discussed, followed by a discussion on the bottom boundary layer and wave effect.

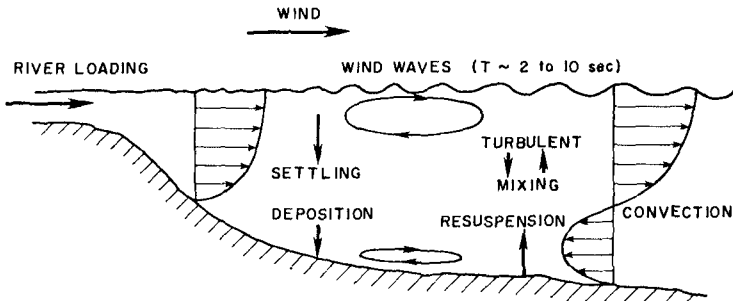


Figure 1. Schematics of Dominant Mechanisms Affecting Sediment Distribution in Shallow Coastal Waters.

A THREE-DIMENSIONAL NUMERICAL MODEL OF COASTAL CURRENTS

In order to study the dynamic response of coastal waters to tides, winds, and meteorological forcing, a three-dimensional, free-surface, time-dependent model is often desired. In addition, stratification and complex topography have to be properly resolved. For relatively long-term application, computational efficiency of the model is extremely important. Traditional three-dimensional, free-surface models (e.g., Leendertse and Liu, 1975) require an exceedingly small time step (associated with the propagation of gravity wave over the distance of a horizontal grid spacing), and hence require extraneous computational costs.

Special features of the present model include (1) a "mode-splitting" procedure which allows efficient computation of the vertical flow structures (internal mode), (2) an efficient ADI scheme for the computation of the vertically-integrated variables (external mode) (3) an implicit scheme for the vertical diffusion terms, (4) a vertically and horizontally stretched coordinate system, and (5) a turbulence parameterization which requires relatively little tuning.

Governing Equations and Boundary Conditions

The basic equations describing the large-scale motion in a large body of water consist of a continuity equation, momentum equations, conservation equations of heat and salinity, and an equation of state. For simplicity here, the last three equations have been combined into an equation for the density. Inherent assumptions are: (1) pressure

distribution is hydrostatic in the vertical direction, (2) Boussinesq approximation is valid, and (3) non-constant eddy viscosities and diffusivities are used to describe the turbulence. The resulting equations are as follows:

$$\frac{\partial u}{\partial x} + \frac{\partial v}{\partial y} + \frac{\partial w}{\partial z} = 0 \quad (1)$$

$$\frac{\partial u}{\partial t} = - \left(\frac{\partial u^2}{\partial x} + \frac{\partial uv}{\partial y} + \frac{\partial uw}{\partial z} \right) + fv - \frac{1}{\rho_0} \frac{\partial p}{\partial x} + \frac{\partial}{\partial z} \left(A_V \frac{\partial u}{\partial z} \right) + \nabla_H \cdot (A_H \nabla_H u) \quad (2)$$

$$\frac{\partial v}{\partial t} = - \left(\frac{\partial uv}{\partial x} + \frac{\partial v^2}{\partial y} + \frac{\partial vw}{\partial z} \right) - fu - \frac{1}{\rho_0} \frac{\partial p}{\partial y} + \frac{\partial}{\partial z} \left(A_V \frac{\partial v}{\partial z} \right) + \nabla_H \cdot (A_H \nabla_H v) \quad (3)$$

$$\frac{\partial p}{\partial z} = - \rho g \quad (4)$$

$$\frac{\partial \rho}{\partial t} = - \frac{\partial u \rho}{\partial x} + \frac{\partial v \rho}{\partial y} + \frac{\partial w \rho}{\partial z} + \frac{\partial}{\partial z} \left(K_V \frac{\partial \rho}{\partial z} \right) + \nabla_H \cdot (K_H \nabla_H \rho) \quad (5)$$

where x and y are the horizontal coordinates; z is the vertical coordinate pointing vertically upward to form a right-handed coordinate system with x and y ; u , v , and w are the three-dimensional velocities in the x , y , and z directions; t is time; f is the Coriolis parameter; g is the gravitational acceleration; p is the pressure; ρ is the density; A_H , and K_H are the horizontal eddy coefficients; A_V and K_V are the vertical eddy coefficients; and

$$\nabla_H \cdot (A_H \nabla_H E) = \frac{\partial}{\partial x} \left(A_H \frac{\partial E}{\partial x} \right) + \frac{\partial}{\partial y} \left(A_H \frac{\partial E}{\partial y} \right) \quad (6)$$

At the free surface, the appropriate boundary conditions are: (a) the wind stress is specified,

$$\rho_0 A_V \left(\frac{\partial u}{\partial z}, \frac{\partial v}{\partial z} \right) = (\tau_{sx}, \tau_{sy}) = \rho_a C_{da} (u_w^2 + v_w^2)^{1/2} (u_w, v_w) \quad (7)$$

where τ_{sx} and τ_{sy} are the wind stresses in the x and y directions respectively, ρ_a is the air density, C_{da} is the drag coefficient and (u_w, v_w) are the wind velocities at a certain height above the surface; (b) the kinematic condition is satisfied,

$$w = \frac{\partial \zeta}{\partial t} + u \frac{\partial \zeta}{\partial x} + v \frac{\partial \zeta}{\partial y} \quad (8)$$

where ζ is the elevation of the free surface; (c) the dynamic condition is satisfied, i.e., $p = p_a$, where p_a is the atmospheric pressure; and (d) the density flux, i.e., the heat flux and the salt flux, is specified.

At the bottom, the boundary conditions are: (a) a quadratic stress law is valid:

$$\rho_0 A v \left(\frac{\partial u}{\partial z}, \frac{\partial v}{\partial z} \right) = (\tau_{bx}, \tau_{by}) = \rho C_d (u_1^2 + v_1^2)^{1/2} (u_1, v_1) \quad (9)$$

where τ_{bx} and τ_{by} are the bottom shear stresses, C_d is the skin-friction coefficient, and (u_1, v_1) are the velocities at the first grid point above the bottom, and (b) heat flux (or temperature) and the salt flux are specified.

Grid Structure

Anticipating appreciable variation of bottom topography in the horizontal direction, the x, y, z coordinate system is vertically-stretched to a x, y, σ coordinate system, such that an equal number of grid points exist in the shallow coastal and the deep offshore areas (Figure 2a). The transformation takes the form:

$$\sigma = \frac{z - \zeta(x, y)}{h(x, y) + \zeta(x, y)} = \frac{z - \zeta}{H} \quad (10)$$

where $h(x, y)$ is the local water depth and $\zeta(x, y)$ is the free-surface

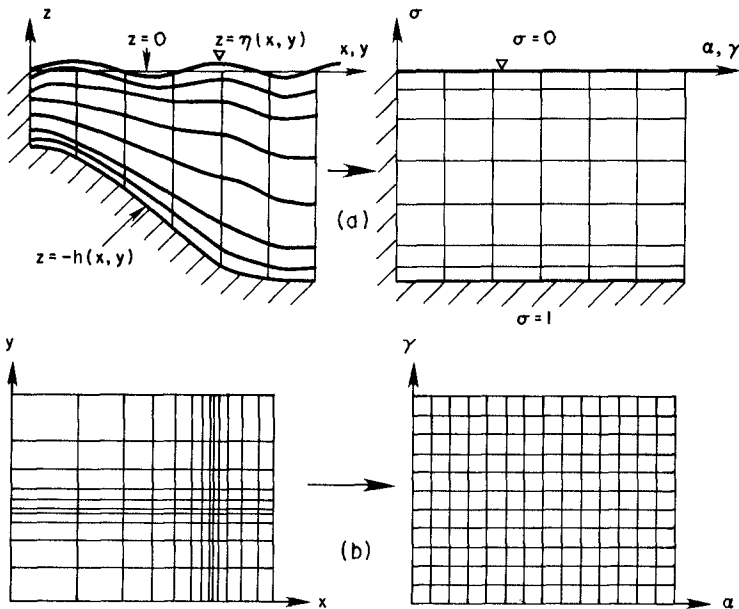


Figure 2(a). Vertical Stretching of the Coordinates,
 (b). Horizontal Stretching of the Coordinates.

elevation. Such a transformation leads to (1) the same order of numerical accuracy in the vertical direction at all horizontal locations, and (2) a smooth representation of the bottom topography. Although additional terms are introduced by this transformation, the advantages warrant its application. Models using regular rectangular grid in the vertical direction cannot accurately resolve the shallow coastal area unless a large number of grid points is used in the deeper offshore area. In addition, if the bottom is approximated by a series of rectangular steps, estimate on bottom stress may be distorted and hence is not suitable for studying sediment transport problems.

To better resolve the complex shoreline geometries and bottom features, a non-uniform grid is often required in the x and y directions (Butler and Sheng, 1982). To allow ease in numerical analysis and as shown in Figure 2b, this non-uniform grid (x,y,z) is further mapped into a uniform grid (α,γ,σ):

$$x = a_x + b_x \alpha^{C_x} ; \quad y = a_y + b_y \gamma^{C_y} \tag{11}$$

The transformed three-dimensional equations of motion in α,γ,σ grid system are rather complex. Detailed equations and boundary conditions in non-dimensional form can be found elsewhere (Sheng, 1981). Staggered numerical grid is used in both the horizontal and vertical directions.

External Mode

In the present study, numerical computation of the vertical flow structures (internal mode), which are governed by slower dynamics, are separated from the computation of the vertically-integrated variables (external mode). This so-called "mode splitting" technique resulted in significant improvement of the numerical efficiency of a three-dimensional hydrodynamic model for Lake Erie (Sheng et al., 1978). It allows for computation of the three-dimensional flow structures with minimal additional cost over computation of the two-dimensional flow with a vertically-integrated model.

The external mode is described by the water level (ζ) and the vertically-integrated mass fluxes (U,V) ≡ ∫_σ⁰ (u,v) H dσ. Performing vertical integration of the transformed three-dimensional equations of motion, and rewriting (α,γ) as (x,y) for simplicity, we obtain:

$$\frac{\partial \zeta}{\partial t} + \frac{1}{\mu_x} \frac{\partial U}{\partial x} + \frac{1}{\mu_y} \frac{\partial V}{\partial y} = 0 \tag{12}$$

$$\begin{aligned} \frac{\partial U}{\partial t} = & - \left[\frac{1}{\mu_x} \frac{\partial}{\partial x} \left(\frac{U^2}{H} \right) + \frac{1}{\mu_y} \frac{\partial}{\partial y} \left(\frac{UV}{H} \right) + H(u_w)_{\sigma=0} \right] - fV - \frac{gH}{\mu_x} \frac{\partial \zeta}{\partial x} + \frac{1}{\rho_0} (\tau_{sx} - \tau_{bx}) \\ & - \frac{1}{\rho_0 \mu_x} \int_{-1}^0 \left[gH \int_{\sigma}^0 \frac{\partial \rho}{\partial x} d\sigma + g \frac{\partial H}{\partial x} \left(\int_{\sigma}^0 \rho d\sigma + \sigma \rho \right) \right] H d\sigma + (H.D.)_x \end{aligned} \tag{13}$$

$$\frac{\partial V}{\partial t} = - \left[\frac{1}{\mu_x} \frac{\partial}{\partial x} \left(\frac{UV}{H} \right) + \frac{1}{\mu_y} \frac{\partial}{\partial y} \left(\frac{V^2}{H} \right) + H(v\omega)_{\sigma=0} \right] + fU - \frac{gH}{\mu_y} \frac{\partial \zeta}{\partial y} + \frac{1}{\rho_0} (\tau_{sy} - \tau_{by}) - \frac{1}{\rho_0 \mu_y} \int_{-1}^0 \left[gH \int_{\sigma}^0 \frac{\partial \rho}{\partial y} d\sigma + g \frac{\partial H}{\partial y} \left(\int_{\sigma}^0 \rho d\sigma + \sigma \rho \right) \right] Hd\sigma + (H.D.)_y \tag{14}$$

where $\mu_x \equiv dx/da$ and $\mu_y \equiv dy/dy$ are the stretching coefficients, $\omega \equiv d\sigma/dt$ is the vertical velocity in the stretched coordinate, and $(H.D.)_x$ and $(H.D.)_y$ are the horizontal diffusion terms. Notice that the bottom stresses (τ_{bx} , τ_{by}) are determined from the latest three-dimensional velocity profiles available from the internal mode computation, and hence are more accurate than the traditional vertically-integrated models which assume the bottom stress is proportional to the local vertically-integrated velocity or its square.

Treating implicitly all the terms in the continuity equation, while only the time derivatives and the surface slopes in the momentum equations, one can obtain the following finite-difference equations:

$$(1 + \phi \lambda_x + \phi \lambda_y) W^{n+1} = [1 + (1 - \phi) \lambda_x + (1 - \phi) \lambda_y] W^n + \Delta t D^n \tag{15}$$

where

$$\lambda_x = \frac{A \Delta t}{\mu_x \Delta x} \delta_x; \quad \lambda_y = \frac{B \Delta t}{\mu_y \Delta y} \delta_y;$$

$$A = \begin{pmatrix} 0 & 1 & 0 \\ gH & 0 & 0 \\ 0 & 0 & 0 \end{pmatrix}; \quad B = \begin{pmatrix} 0 & 0 & 1 \\ 0 & 0 & 0 \\ gH & 0 & 0 \end{pmatrix}; \quad D = \begin{pmatrix} 0 \\ D_x \\ D_y \end{pmatrix}; \quad W = \begin{pmatrix} \zeta \\ u \\ v \end{pmatrix} \tag{16}$$

where $(\Delta x, \Delta y)$ are the spatial grids, Δt is time step, D_x and D_y are terms in Eqs. (13) and (14) excluding the time derivatives and the surface slopes, superscripts $n+1$ and n indicate present and previous time step of integration, δ_x and δ_y are central difference spatial operators, and ϕ is a weighting factor, $0 < \phi < 1$. If $\phi = 0$, Eq. (15) reduces to a two-step explicit scheme. If $\phi > 0$ the resulting schemes are implicit, with $\phi = 1/2$ corresponding to the Crank-Nicholson scheme and $\phi = 1$ corresponding to the fully implicit scheme. Eq. (15) can be factorized such that solution can be obtained by consecutive tridiagonal matrix inversions in the x-direction and y-direction. Further, we employ a method that solves only two variables during each sweep. This method allows very large time step to be used and has been found to be more stable than the traditional ADI method. Courant number based on the maximum propagation speed of surface gravity wave, $(gH_{max})^{1/2} \Delta t / \Delta x$, may now be as large as 100, compared to the limit of 1 for the explicit method. The maximum step is now governed by the CFL condition based on vertically-averaged advection speed in the system.

In the full three-dimensional model, the external mode computation

is carried out in conjunction with the internal mode computation. Depending on the problem of interest, the internal mode may be computed every so often with a time step equal to or greater than the external time step.

Internal Mode

The internal mode of the flow is described by the vertical flow structures and the density. Defining perturbation velocities as $u' \equiv u - U/H$ and $v' \equiv v - V/H$, the equations for the internal mode are obtained by subtracting the vertically-averaged momentum equations from the three-dimensional equations:

$$\frac{1}{H} \frac{\partial Hu'}{\partial t} = B_x - \frac{D_x}{H} + \frac{1}{H^2} \frac{\partial}{\partial \sigma} \left[A_v \frac{\partial}{\partial \sigma} \left(\frac{Hu' + U}{H} \right) \right] \quad (17)$$

$$\frac{1}{H} \frac{\partial Hv'}{\partial t} = B_y - \frac{D_y}{H} + \frac{1}{H^2} \frac{\partial}{\partial \sigma} \left[A_v \frac{\partial}{\partial \sigma} \left(\frac{Hv' + V}{H} \right) \right] \quad (18)$$

where B_x and B_y represent all terms in the transformed three-dimensional momentum equations except the surface slopes and the vertical diffusion terms, and D_x and D_y are defined in Eq. (16). Notice that the above equations retain the three-dimensionality and hence are different from the model of Nihoul and Roday (1983) which is actually a superposition of a two-dimensional model and a vertical one-dimensional model.

The above equations do not contain the surface slope terms and hence a large time step may be used in the numerical computation. In the present model, a two-time-level or three-time-level scheme with a vertically implicit scheme is generally used. The bottom friction terms are also treated implicitly to ensure unconditional numerical stability in shallow waters. Care must be taken to ensure that the vertically-integrated perturbation velocities at each horizontal location (i,j) always equal to zero.

Once the equations for (u',v') are solved, and (u,v) obtained, vertical velocity ω and density ρ may be computed. As mentioned before, the internal mode may be computed as often as the external mode or as desired and as dictated by the problems of interest. The numerical time step for the internal mode is limited by the CFL condition based on the advection speed. In the present study, the drag coefficient C_d in the quadratic bottom stress law Eq. (9) is generally specified as a function of the bottom roughness (z_0), the distance above the bottom (z), at which (u_1, v_1) is computed, and the stability function of the bottom flow (ϕ_s):

$$C_d = k^2 \left(\lambda n \frac{z_1}{z_0} + \phi_s \right)^{-2} \quad (19)$$

where k is the von Karman constant. It can be shown that the stability may increase (unstable case) or decrease (stable case) the drag

coefficient by as much as 40% (Sheng, 1980).

Turbulence Parameterization

A semi-empirical theory of vertical mixing is used in this study. The effect of stratification, as measured by the Richardson number, Ri, on the intensity of vertical turbulent mixing is parameterized by a number of empirical stability functions:

$$A_v = A_{v0} \phi_1 (Ri); \quad K_v = K_{v0} \phi_2 (Ri); \quad Ri = \frac{-g}{\rho} \frac{\partial \rho}{\partial z} \left[\left(\frac{\partial u}{\partial z} \right)^2 + \left(\frac{\partial v}{\partial z} \right)^2 \right]^{-1/2} \quad (20)$$

where A_{v0} and K_{v0} are the eddy coefficients in the absence of any density stratification and ϕ_1 and ϕ_2 are stability functions. Traditionally, these stability functions have been determined empirically by comparing model output with measured data. As shown in Figure 3a, great discrepancy exists among the various empirical forms of the stability functions. In addition, the critical Richardson numbers, at which turbulence is completely damped by buoyancy, given by these formulas are much too high (10) compared to the measured value of 0.25 (Erikson, 1978). To unify this discrepancy, stability functions may be determined from a second-order closure model of turbulence. Assuming a balance between turbulence production and dissipation, i.e., the so-called "super-equilibrium" condition (Donaldson, 1973), we can obtain a simpler set of algebraic relationships between the turbulent correlations and mean flow gradients. As shown in Figure 3b, such a stability function leads to a

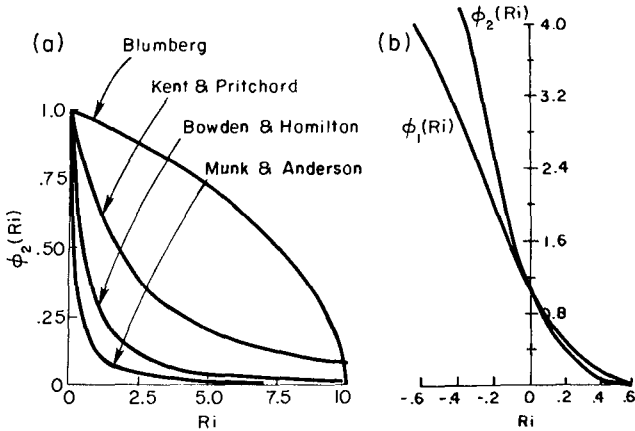


Figure 3. Stability Function vs. Richardson Number:
 (a). Empirical Formulations,
 (b). "Superequilibrium" Formulation Derived from Reynolds Stress Model.

critical Richardson number much closer to 0.25. In addition, such a formulation allows the definition of finite eddy coefficients in the unstable range ($Ri < 0$). In order to utilize these relationships, a turbulence length scale which varies with depth and Richardson number has to be prescribed empirically.

SIMULATION OF TIDE- AND WIND DRIVEN CURRENTS

The three-dimensional numerical model of coastal currents has been applied to simulate the tide- and wind-driven currents in the Mississippi Sound and adjacent continental shelf waters of the Gulf of Mexico. As shown in Figure 4, the horizontal grid is composed of 116 grid points in the y-direction and 60 grid points in the x-direction. The smallest grid spacing in the computational domain is on the order of 1 km. The water depth varies from only a few meters within the Mississippi Sound and the Mobile Bay to over 1000 m along the southern boundary.



Figure 4. Computational Grid for Mississippi Sound Simulation.

Tides in the Gulf of Mexico

Gulf tides differ from tides in most other places in the world due to the dominance of the diurnal components K1, O1 and P1 collectively over the semi-diurnal components M2 and S2, except along the west Florida coast. Reid and Whitaker (1981) developed a numerical tide model for the Gulf based on the vertically-integrated, linearized tidal equations to portray the barotropic response of the Gulf to tidal forcing. Forcing at ports was also included with an impedance type condition. Detailed data from 20 tidal gages located in open coastal

waters of the Gulf were used for the fine tuning of their model. Their study confirmed that diurnal tide in the Gulf is primarily a co-oscillating tide driven by adjoining Atlantic Ocean and Caribbean Sea.

The water level response for a given tidal constituent is usually expressed in terms of the surface displacement ζ (Schureman, 1941):

$$\zeta = F(t) A(\lambda, \phi) \cos [\omega_0 t + \chi - G(\lambda, \phi)] \quad (21)$$

where λ is the longitude, ϕ is the latitude, A is the mean amplitude over 18.6 years and G the Greenwich phase or epoch at given position (λ, ϕ), ω_0 is tidal frequency, χ is the astronomical argument, while F is the nodal factor, a slowly varying function of time. Tides at particular stations are characterized by A and G for individual constituents. In our study, A 's and G 's for 5 constituents (O1, K1, P1, S2 and M2) along the open boundaries of our grid are supplied from Reid and Whitaker's model. Surface displacements at the open boundary stations are determined from a linear combination of those due to the five tidal constituents.

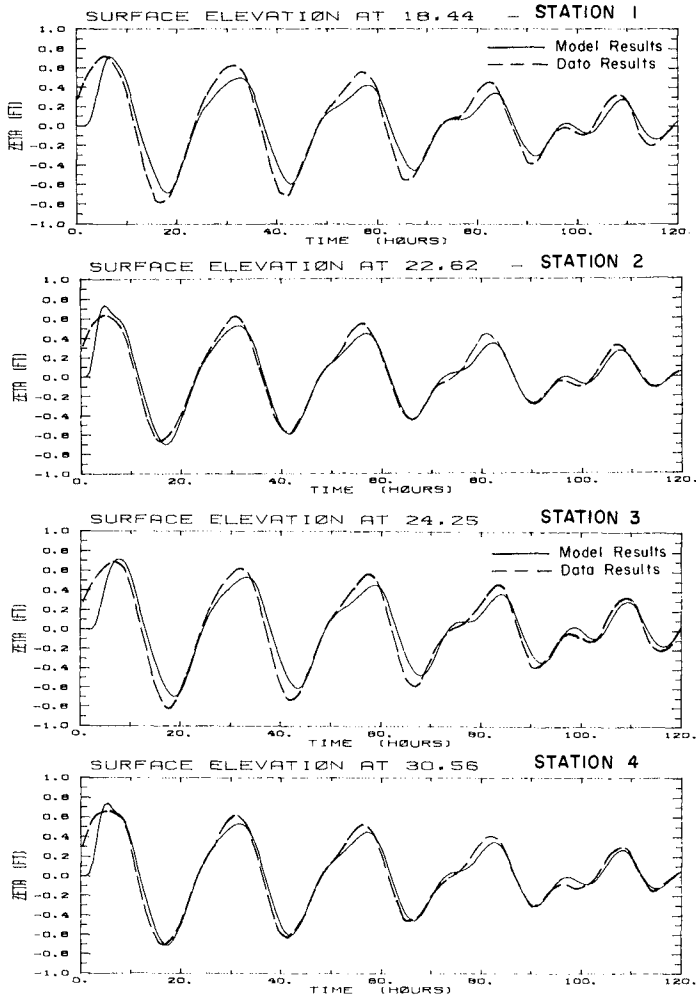
Tidal Currents off the Mississippi Coast

As a first example, tides during 20 Sept. to 25 Sept. 1980 are computed with our three-dimensional model. The surface displacements at four stations (see Figure 4 for locations) within the Mississippi sound are compared with measured data in Figure 5. Notice that the measured data have been filtered such that variations due to short-period oscillations on the order of a few hours or less are not included. Initially, the diurnal tides are predominant. Towards the end of the five-day period, the diurnal tides become somewhat less predominant while the semi-diurnal tides became gradually more apparent. Good agreement is found at all stations.

In this simulation, a relatively large time step of 12 minutes was used for both the external and the internal modes. Seven grid points are used in the vertical direction. A relatively smooth bottom with a roughness length, z_0 , of 0.1 cm was assumed. A parabolic length scale, Λ , was assumed in the vertical direction.

The tide-driven horizontal currents at mid-depth are shown in Figure 6 for two stations in the Mississippi Sound. Currents on the order of 30 cm/sec exist at both stations. Again, reasonable agreement is found between data and model results.

The horizontal velocity field at 1 m depth, after 3 days of simulation, is shown in Figure 7. Relatively large currents exist at the various tidal inlets and in the area between the Ship Island and the Chandelier Island. Except in these areas, at this instant of time, bottom shear stress generated by the tidal currents are generally less than 0.8 dyne/cm². Hence little sediment resuspension is expected. However, during strong spring tides, such as those during the period of 12 June to 16 June, 1980, relatively stronger currents and bottom shear stresses in excess of 0.8 dyne/cm² could prevail within the tidal



20 SEPT., 1980

25 SEPT., 1980

Figure 5. Surface Elevation at Four Locations (see Fig. 4) from 20 Sept. to 25 Sept., 1980.

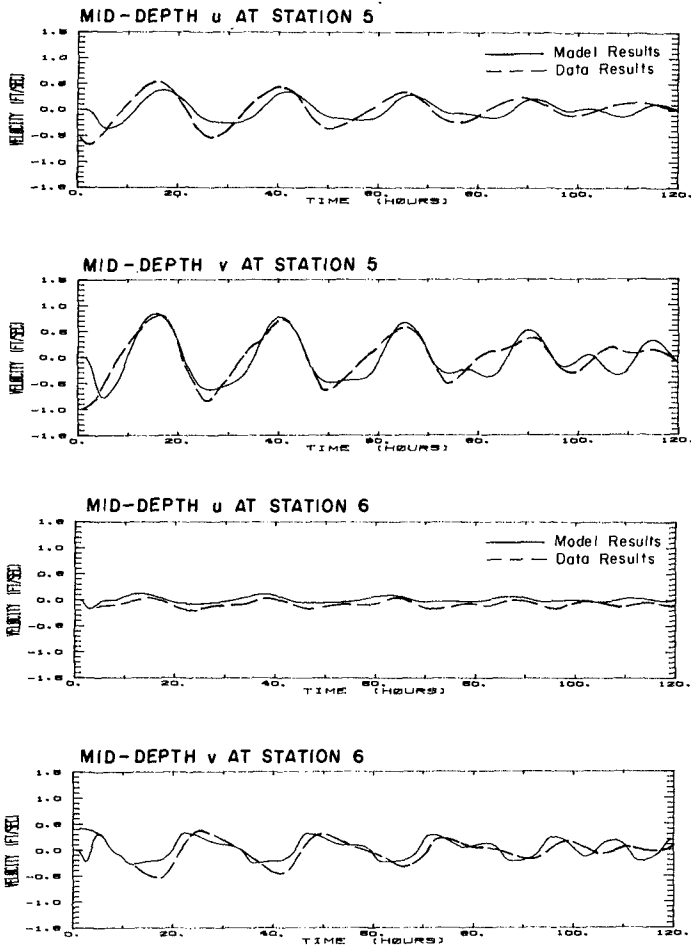


Figure 6. Mid-Depth Horizontal Velocities at Stations 5 and 6 from 20 Sept. to 25 Sept., 1980. Tide Forcing Only.

inlets and other shallow areas. Resuspension of cohesive sediment in these areas might occur and leave behind the coarser non-cohesive sediment.

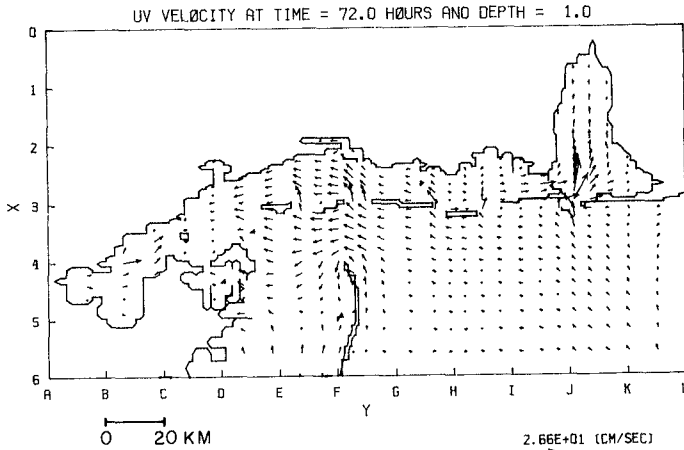


Figure 7. Tide-Driven Horizontal Velocities at 1 m Depth in the Vicinity of the Mississippi Sound at 0 hr, 23 Sept., 1980.

Wind-Driven Currents off the Mississippi Coast

The results presented in the above did not contain any wind-driven effect. During our study, wind data were collected at several meteorological stations surrounding the Mississippi Sound. The wind during the 5-day period was generally quite mild (≤ 5 m/sec) from the Southeast. To examine the effect of wind on the currents, we carried out a three-day simulation from 20 Sept., using a uniform wind stress of 1 dyne/cm^2 from the Southeast. The southeasterly wind caused water to pile up within the Mississippi Sound, with a set-up on the order of 12 cm along the Northern shore, and only 6 cm behind the barrier islands.

The influence of wind on the current also depends on the location. Figure 8 shows the along-shore velocity at 2 locations over the 3-day period. At Station 5, off Cat Island, the presence of the wind did not have appreciable effect on the tidal current. At Station 6, within the pass between the Mississippi Sound and the Mobile Bay, the wind caused significant flow from the Mobil Bay into the Sound. This resulted in a significantly larger bottom shear stress which leads to the reduction in the amplitude of the tidal currents.

Wind-driven currents in the Mississippi Sound depend strongly on the wind direction. For example, assuming a uniform wind stress of 1 dyne/cm^2 from the West, our model results showed relatively stronger currents in the along-shore direction (Figure 9). Notice the near-surface and near-bottom velocities differ not only in magnitude but also in direction at some locations. This is partially associated

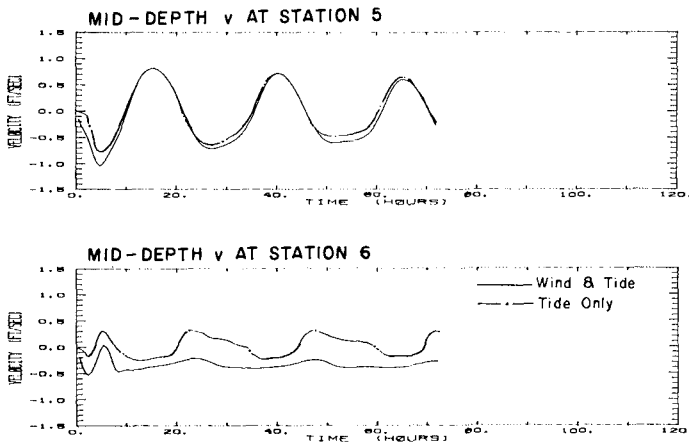


Figure 8. Mid-Depth Along-Shore Velocity at Stations 5 and 6 from 20 Sept. to 23 Sept., 1980. Tide and Wind Forcings.

with the pressure gradient caused by the wind set-up, which is on the order of 20 cm across the Mississippi Sound. According to a laboratory flume study on the erodibility of the Mississippi Sound sediments (Sheng, 1981), it is expected that the bottom shear stress generated by the strong Westerly wind in winter may cause significant resuspension of sediments.

TRANSPORT, RESUSPENSION, AND DEPOSITION OF COHESIVE SEDIMENTS

Transport Modes

The transport of cohesive sediment in the water column can be described by a conservation equation, similar to the heat or salinity equation, for the suspended sediment concentration. An equation similar to Eq. (5) can be written for the sediment concentration C . However, the vertical velocity in the sediment concentration equation should be composed of the sum of the fluid velocity (w) and a settling speed of the particles (w_s). In fresh water, the settling speed of cohesive sediment from a coastal environment shows a relatively flat spectral distribution. As the salinity increases, the sediment particles form aggregates and the spectral distribution becomes much sharper (Fig. 10). In this study, for simplicity, we assume the cohesive sediment in the Mississippi Sound can be described by one single settling speed. The settling speed of bottom sediment samples from the Sound was measured in laboratory, without adding dispersant to the samples, and a median settling speed determined.

The behavior of sediment in the water column depends on the

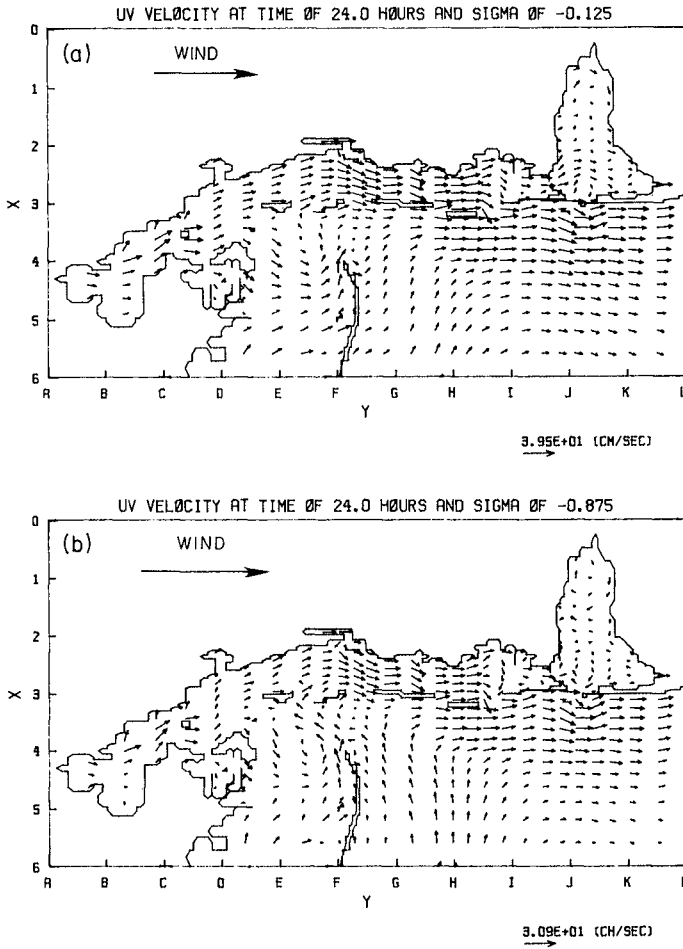


Figure 9. Horizontal Velocities in the Vicinity of the Mississippi Sound at 24 hrs after the Application of a Westerly Wind with $\tau_y = 1.0$ dyne/cm².
 (a). Near-Surface Currents, and
 (b). Near-bottom Currents.

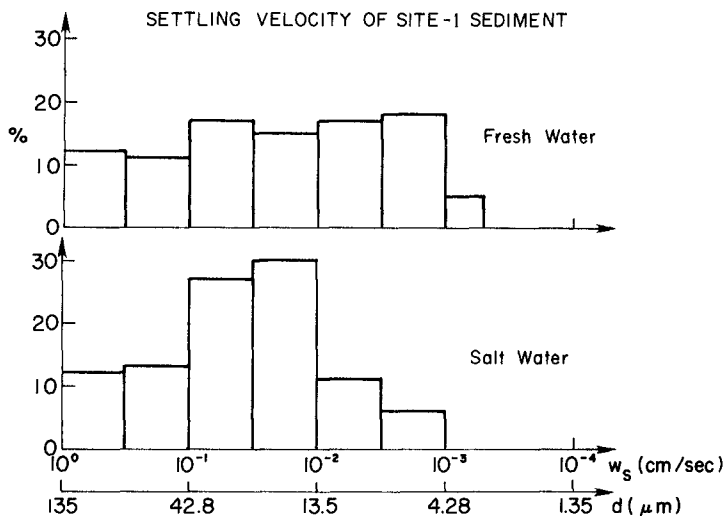


Figure 10. Settling speed of Mississippi Sound Sediments in Fresh and Salt Water.

cohesion and collision of sediment particles. Clay mineralogy and other chemical parameters determine the cohesion of sediment particles. However, in coastal waters where flow is generally turbulent, collision between particles play a more dominant role than cohesion in determining the state of flocculation. The frequency of collision between various groups of particles depends on the turbulent shearing rate on the dissipation scale and differential settling. Although our hydrodynamic model is capable of computing the small-scale turbulent shearing rate, there is insufficient data at this time to allow for precise determination of model coefficients for the flocculation model.

Resuspension and Deposition Modes

Resuspension and deposition of sediment at the sediment-water interface play important roles in the distribution of suspended sediment concentration. In general, resuspension and deposition depend on (1) the hydrodynamic forces generated at the bed within the turbulent bottom boundary layer; (2) bed properties such as sediment composition, water content, bed preparation (settling) time, and organic matter, bacteria, and benthos; and (3) fluid properties including salinity, temperature, and pH of pore water and overlying water.

Effects of dominant parameters (shear stress, water content, bed preparation time, and salinity) on resuspension and deposition were

investigated in a laboratory flume (Sheng 1981; Sheng et al. 1982). To prepare the bed, sediments are introduced into the flume, resuspended, and allowed to settle for a period of 1 to 10 days. A given bottom shear stress is then applied and the time history of sediment concentration recorded until an equilibrium concentration is reached, at which the resuspension balances the deposition. As shown in Figure 11, resuspension as indicated by the equilibrium concentration depends strongly on the applied shear stress. More than an order of magnitude increase in equilibrium concentration can be expected when the shear stress is increased by a factor of 5. Salinity affects the aggregation of particles and hence the erodability of the

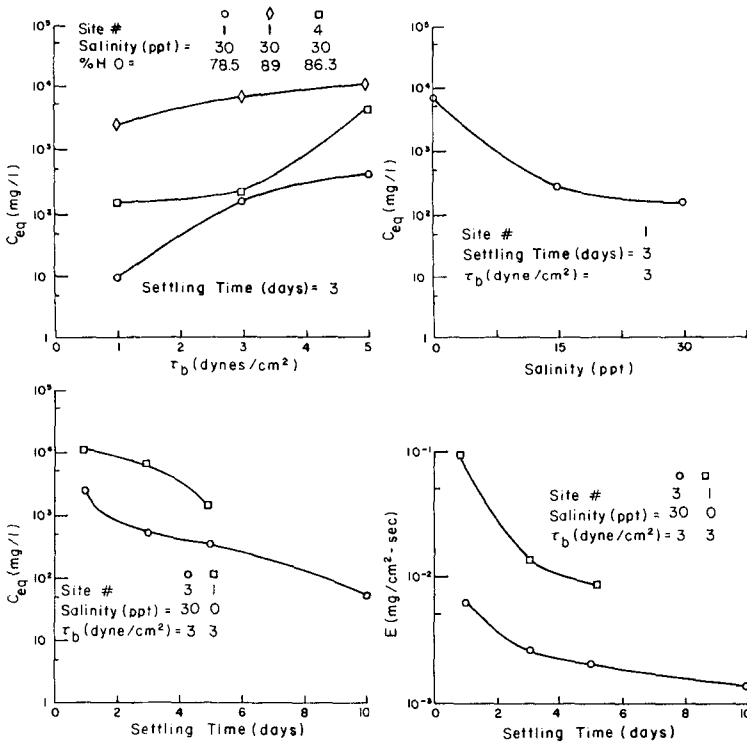


Figure 11(a). Equilibrium Suspended Sediment Concentration in Laboratory Flume as a Function of Applied Shear Stress, (b). Effect of Salinity, (c). Effect of Time History of the Bed, and (d). Resuspension Rate as a Function of Time History of the Bed.

bottom sediments. The sediment becomes harder to erode at higher salinity, with most variation occurring between 0 and 15 ‰. The sediment also becomes harder to erode as more time is allowed for the preparation of the bed. From the laboratory flume data, proper bottom boundary conditions for the sediment transport model can be derived in terms of the rate of resuspension (E) and deposition ($V_d C$) (Sheng, 1981). The bottom boundary condition for the sediment concentration (C) equation can be written as:

$$\text{Net Upward Flux} = w_s C - K_v \frac{\partial C}{\partial z} = E - V_d C \quad (22)$$

where the deposition velocity $V_d > 0$ while the settling velocity $w_s < 0$.

Sediment Movement in the Mississippi Sound Due to a Westerly Wind

As an example to illustrate the important role of resuspension and deposition, we performed a 1-day simulation of sediment movement due to a Westerly wind.

Initially, the background concentration is assumed to be zero everywhere except within a square area (shown in Figure 12) where the concentration is 500 mg/l (newly introduced sediment). The sediment concentration is then computed with three different bottom boundary conditions: (1) zero net flux and zero settling speed, (2) with deposition and resuspension, but no resuspension of old sediment (vs. the newly introduced sediment) is allowed, and (3) deposition and resuspension allowed at all locations. For (2) and (3), a settling

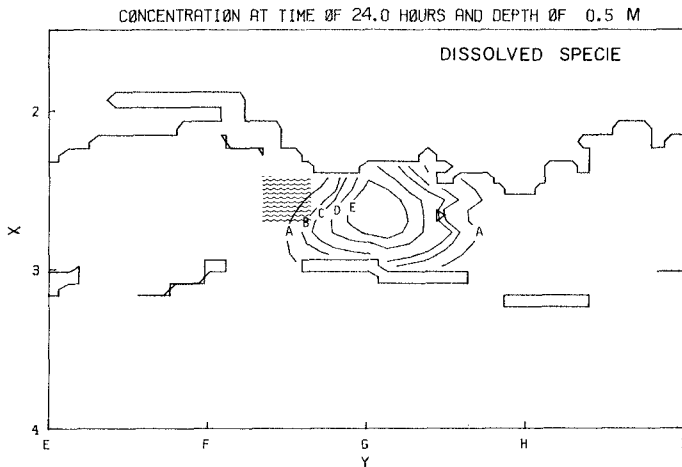


Figure 12. Suspended Sediment Concentration at 0.5 m Depth at the End of 1-day Simulation. Westerly Wind; No Settling; Zero Net Flux at Bottom.

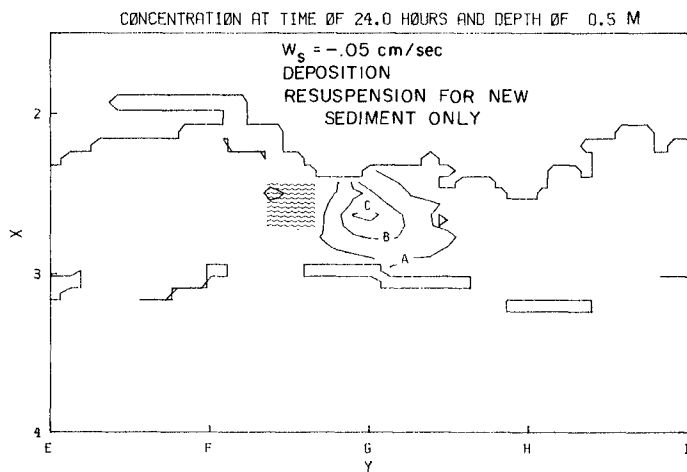


Figure 13. Same as Figure 12 except that $w_s = -0.05 \text{ cm/sec}$; Deposition but no Resuspension for Old Sediment.

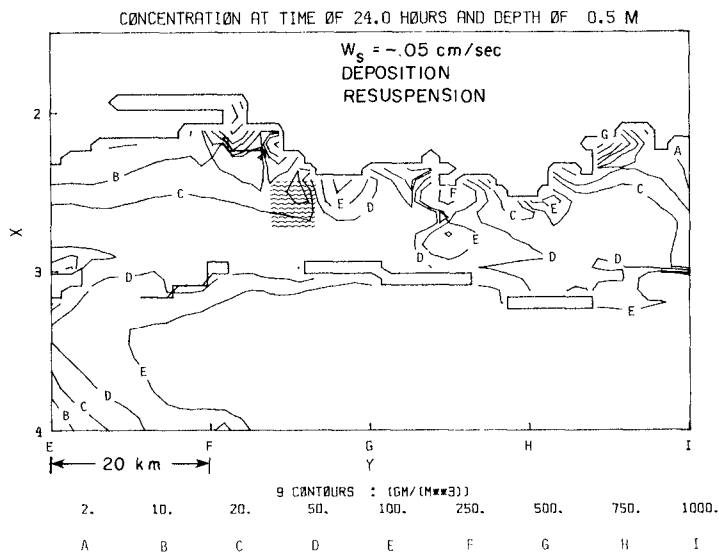


Figure 14. Same as Figure 12 except that $w_s = -0.05 \text{ cm/sec}$; Deposition and Resuspension.

speed of 0.05 cm/sec was used. The results at 0.5 m depth at the end of one-day simulation are shown in Figures 12, 13 and 14. It is clear that resuspension of sediment plays a dominant role in redistributing sediment. The difference in results for (2) and (3) reflects the importance of quantifying the time history of bottom sediments, which strongly affects the erodability as shown in Fig. 11.

BOTTOM BOUNDARY LAYER AND WAVE EFFECT ON SEDIMENT RESUSPENSION

The wave climate during the September period of 1980 was studied by means of a spectral wave hindcasting model modified for shallow water. The blockage effect of the barrier islands allows us to assume that most of the wave energy in the Mississippi Sound was derived from the wind fetch within the Sound. From 20 to 25 Sept., wind was generally from the Southeast at about 5 m/sec. Results of the wave model indicate wave height generally under 30 cm and wave period under 3 sec. At a station off Gulfport (Station 17), the wave-induced bottom stress was the highest among all stations and on the order of 5 dyne/cm² during the first day (Fig. 15a). However, wave-induced stress over most of the sound was generally not very strong, as can be seen in Fig. 15b, the bottom stress at a station off the Biloxi channel (Station 10) was generally less than 1.3 dyne/cm². These findings are consistent with the sediment concentration data collected during this time period, which showed a slight initial increase in concentration followed by primarily depositional events. We also found that linear wave theory and empirical bottom stress formula tend to overestimate the wave-induced bottom stress within an oscillatory boundary layer.

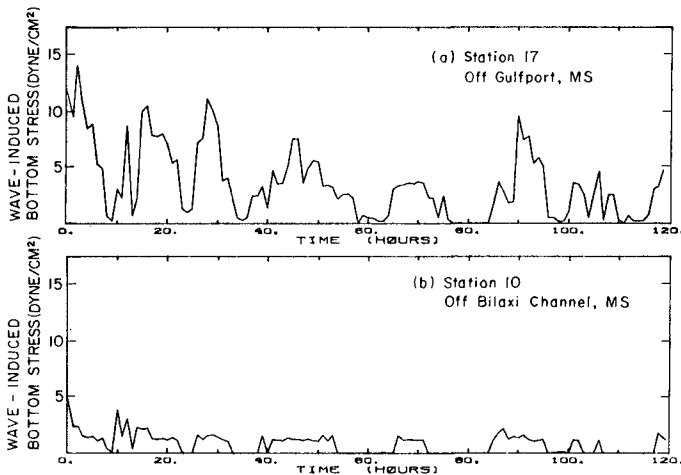


Figure 15. Wave-Induced Bottom Stress at two Locations in the Mississippi Sound from 20 to 25 Sept., 1980.

- (a). Station 17 off Gulfport, MS.
- (b). Station 10 off Biloxi Channel.

Detailed turbulent dynamics of the bottom boundary layer under a pure wave (Sheng, 1982) and current-wave interaction (Sheng and Lewellen, 1982) have also been studied using a Reynolds stress model. Contrary to the general belief, the presence of the wave was found to not always enhance the current-induced stress.

CONCLUSIONS AND RECOMMENATIONS

An efficient three-dimensional numerical model of coastal currents has been developed and is operational. The model is suitable for detailed short-term simulations as well as longer-term simulations. Currents in Mississippi Sound and adjacent offshore waters have been computed with the three-dimensional model. Results obtained during a five-day period in September 1980 agree very well with the measured data. Large spatial and temporal variation of bottom shear stresses exist within the area. Rate of resuspension of the Mississippi Sound sediments (primarily Smectite) has been determined experimentally and was found to increase with increasing shear stress, decreasing salinity, and shorter time-history of the bottom sediment. Studies are needed to elucidate the effect of turbulence on flocculation, the current-wave interaction within the bottom boundary layer, and the inclusion of sediment time-history as a parameter in the mathematical model.

ACKNOWLEDGEMENT

This work is supported by the U.S. Army Engineer Waterways Experiment Station under contract OACW 39-80-C-0087. Permission was granted by the Army Chief of Engineers to publish this information. Richard Schmalz and Bob Jensen provided valuable assistance in the study.

References

- Blumberg, A.F., 1975: "A Numerical Investigation into the Dynamics of Estuarine Circulation," Chesapeake Bay Institute Report No. 91, Baltimore, MO.
- Bowden, K.F. and P. Hamilton, 1975: "Some Experiments with a Numerical Model of Circulation and Mixing in a Tidal Estuary," Estuarine Coastal Marine Sci., 3, 281.
- Butler, H.L. and Y.P. Sheng, 1982: "ADI Procedures for Solving the Shallow-Water Equations in Transformed Coordinates," Proc. 1982 Army Num. Anal. and Comp. Conf., Army Research Office, pp. 365-380.
- Oonaldson, C.duP., 1973: "Atmospheric Turbulence and the Dispersal of Atmospheric Pollutants," in AMS Workshop on Micrometeorology (D.A. Haugen, ed.), Science Press, Boston, pp. 313-390.
- Erikson, C.C., 1978: "Measurements and Models of Fine Structure, Internal Gravity Waves and Wave Breaking in the Deep Ocean," J. Geophys. Res., 83, pp. 2989-3009.

- Kent, R.E., and D.W. Pritchard, 1959: "A Test of Mixing Length Theories in a Coastal Plain Estuary," J. Mar. Res., 18, pp. 62-72.
- Leendertse, J.J., and S.K. Liu, 1975: "A Three-Dimensional Model for Estuaries and Coastal Seas, II: Aspects of Computation," Rand Report R-1764-OWRT.
- Munk, W.H. and E.P. Anderson, 1948: "Notes on the Theory of the Thermocline," J. Mar. Res., 1, pp. 276-295.
- Nihoul, J.C.J. and F.C. Roday, 1983: "Three-Dimensional Marine Models for Impact Studies," Proc. 18th Int'l Conf. Coastal Eng., This Volume.
- Reid, R.O. and R.E. Whitaker, 1976: "Wind-Driven Flow of Water Influenced By a Canopy," J. Waterways, Harbors and Coastal Eng. Div., Proc. ASCE, pp. 63-77.
- Schureman, P. 1941: "Manual of Harmonic Analysis and Prediction of Tides," U.S. Department of Commerce Special Pub. No. 98, 317 pp.
- Sheng, Y.P., 1980: "Modeling Sediment Transport in a Shallow Lake," in Estuaries and Wetland Processes (P. Hamilton, ed.), Springer-Verlag, Berlin, Heidelberg, pp. 299-337.
- Sheng, Y.P., 1981: "Modeling the Hydrodynamics and Dispersion of Sediments in the Mississippi Sound," A.R.A.P. Report No. 455, 107 pp.
- Sheng, Y.P., 1982: "Hydraulic Applications of a Second-Order Closure Model of Turbulent Transport," in Applying Research to Hydraulic Practice, (P. Smith, Ed.), ASCE, pp. 106-119.
- Sheng, Y.P. and W.S. Lewellen, 1982: "Current and Wave Interaction within the Benthic Boundary Layer," EOS, 63, 3, pp. 72-73.
- Sheng, Y.P. and W. Lick, 1979: "The Transport and Resuspension of Sediments in a Shallow Lake," J. Geophys. Res., 84, C4, 1809-1826.
- Sheng, Y.P., W. Lick, R. Gedney, and F. Molls, 1978: "Numerical Computation of the Three-Dimensional Circulation in Lake Erie; A Comparison of a Free-Surface and a Rigid-Lid Model," J. Phys. Ocean., 8, pp. 713-727.
- Sheng, Y.P., P.L. McCall, and J.B. Fisher, 1982: "Entrainment of Cohesive Sediments of the Gulf of Mexico," EOS, 63, 18, p. 358.